ISSN 0036-0236, Russian Journal of Inorganic Chemistry, 2022, Vol. 67, No. 8, pp. 1324–1337. © Pleiades Publishing, Ltd., 2022.
ISSN 0036-0236, Russian Journal of Inorganic Chemistry, 2022. © Pleiades Publishing, Ltd., 2022.

INORGANIC MATERIALS AND NANOMATERIALS

One-Pot Sol-Gel Synthesis of Doped TiO_2 Nanostructures for Photocatalytic Dye Decoloration

J. Sakfali[a], *, S. Ben Chaabene[a], R. Akkari[a], and M. Said Zina[a]

[a] *Université de Tunis El Manar, Faculté des Sciences de Tunis, Laboratoire de Chimie des Matériaux et Catalyse, Tunis, 2092 Tunisie*

**e-mail: jamila.sakfali@fst.utm.tn*

Received January 9, 2022; revised March 9, 2022; accepted March 25, 2022

Abstract—In this work, a series of TiO_2 nanostructures doped with well-selected transition metals (Cr, Fe, Co and Zr) was prepared using a simple "one-pot" sol-gel process, followed by a drying under supercritical conditions of solvent. Herein, we carefully highlighted the effect of doping with ions exhibiting higher size than that of Ti^{4+} host ion, on physicochemical properties of TiO_2 aerogel nanomaterials, and its photocatalytic behavior in the methylene blue degradation under solar light irradiation. Textural properties revealed materials with high surface areas given by supercritical drying process. TEM analysis of pristine oxide showed quantum-sized, well-dispersed and highly ordered particles. XRD analysis evidenced an increase in anatase lattice volume after doping. A reduction in gap energy can be seen for Cr, Fe and Co doped TiO_2 samples, which is related to the involvement of intermediate energy levels related to dopant ions. Photocatalytic activity of TiO_2 solid shows an apparent improvement when doped with zirconium compared to other doped TiO_2 materials and pristine oxide, which may be mainly correlated to the increase in the amount of oxygen defects given its larger size as shown by PL spectroscopy. Oxygen vacancies act as electron traps thus provide a charge separation enhancing the photoactivity. The low photoactivity of $Cr–TiO_2$, $Fe–TiO_2$, and $Co–TiO_2$ materials was mainly related to the dopant energy levels appearing as charge recombination centers, which can negatively affect the catalytic efficiency. Hence, the efficiency of photocatalysis seems determined by the competition between these two process; charge separation and charge recombination.

Keywords: TiO_2 photocatalyst, sol-gel "one-pot," aerogel, transition metal doping, oxygen vacancies

DOI: 10.1134/S003602362208023X

INTRODUCTION

Environmental pollution has become a standout amongst the most difficult issues facing humanity and other forms of life on our planet today. Thus, chemical pollutants contaminate water, air and soil, endangering human health and threatening ecosystems [1–3]. Water pollution in a huge part of the planet is attracting increasing attention from specialists around the world, pushing them to find solutions to this issue [4, 5]. In particular, textile industries pollute water sources, because of the irregular use and release of different kinds of dyes [6]. Several processes are implemented to eliminate or reduce the harmful effects of water pollutants, such as the advanced oxidation processes (AOPs), which are environmentally friendly and hygienic depolluting technologies. AOPs are practically efficient and promising for the treatment of various toxic and organic pollutants and the complete destruction of contaminants of emerging concern such as pesticides, dyes, pharmaceutical compounds and other harmful contaminants [7]. AOPs are essentially based on the production of powerful oxidizing agents that react non-selectively with most organic compounds, degrading even the most recalcitrant ones. Among AOPs, heterogeneous photocatalysis in the presence of titanium dioxide TiO_2 has proven to be a promising technology for the degradation of organic pollutants with high removal and mineralization rates compared to other AOPs. This "green" process is based on the generation of highly reactive oxygen species ($OH^{\bullet}$, $O_2^{\bullet-}$) by photoexcitation of a semiconductor, absorbing energy radiation equal to or greater than its gap energy. These highly oxidizing species react with organic compounds, the redox reactions are responsible for the destruction of pollutants [8]. Titanium dioxide TiO_2 nanomaterials have been widely studied over the last two decades due to their attractive properties and potential applications [9]. TiO_2 has proven to be an ideal photocatalyst because of its many advantages such as photostability, chemical inertness, non-toxicity and relatively low cost [10–12]. However, its catalytic activity limited to the UV region and the rapid recombination of electron-hole charges restrain its efficiency [13]. TiO_2 is active in the UV region ($\lambda <$ 400 nm) which represents 3 to 5% of the sunlight reaching the earth, from an energy point of view, these

radiations are not profitable [13]. To overcome this problem, doping TiO_2 with metallic [14–16] and non-metallic [17–19] elements has proved to be an alternative that may improve the photocatalytic activity of titania by decreasing the band gap and thus extending its absorption to the visible region, and by reducing the recombination of photogenerated charges. Various methods can be used for the preparation of TiO_2 such as precipitation [20], hydrothermal [21], electrochemistry [22], microemulsion [23] and deposition [24]. The optimization of the catalyst requires its synthesis in nanometric form, this requirement explains the sol-gel approach used in this work. The sol-gel process was used because of its simple, easy, flexible and highly efficient operating conditions. This process enables the elaboration of a wide variety of oxides of different forms (powders, thin films, fibers, etc.). It also has the ability to control a large number of parameters such as homogeneity, purity, porosity and particle size [25].

We report in this work the effect of doping TiO_2 with a series of transition metals : chromium, iron, cobalt and zirconium, using a simple "one-pot" sol-gel method followed by a supercritical drying of solvent. The method of preparation as well as the drying process are hardly used in the literature, hence the originality of the work. Specifically, the effect of dopant ions having higher size (ionic radii) than the Ti^{4+} host ion (Ti^{4+} (74.5 pm) < Cr^{3+} (75.5 pm) < Fe^{3+} (78.5 pm) < Co^{2+} (79 pm) < Zr^{4+} (86 pm)), on physicochemical properties and photocatalytic activity of titanium oxide is studied. The catalytic performance of synthesized photocatalysts were evaluated in the photodegradation reaction of the methylene blue (MB), a toxic dye posing a real problem of water contamination generated by the activity of textile industries. The methylene blue dye has been the subject of several research projects around the world as a pollutant model, the research teams have tried to degrade it using various methods [26–29] especially over doped TiO_2 catalysts prepared via different methods. They have shown that cationic doping with transition metals improves the catalytic activity of TiO_2 in several cases [30–33]. However, in other cases, the doping resulted in a hampered efficiency of the TiO_2 photocatalyst [34–37]. To the best of our knowledge, few comparative studies, based on our approach and relating the photodegradation of methylene blue dye over TiO_2 solids doped with selected transition metals, has been described in the literature. Subsequently, the materials obtained were characterized by means of X-ray diffraction, High resolution transmission electron microscopy, Nitrogen physisorption at 77K, UV-Vis diffuse reflectance spectroscopy and photoluminescence spectroscopy. Finally, the performances of the catalysts were discussed.

EXPERIMENTAL

Materials. Titanium(IV) isopropoxide (97%, Aldrich), cobalt nitrate (97%, LOBA Chemie), zirconyl nitrate (99.5%, LOBA Chemie), chromium nitrate (99%, Sigma-Aldrich) and iron nitrate (98%, Sigma-Aldrich) have been used as sources of titanium, cobalt, zirconium, chromium and iron, respectively, for the preparation of doped nanomaterials. Isopropyl alchool (99.5%, Acros) was used as a solvent. Ethyl acetoacetate (98%, Fluka) and nitric acid (65%, Scharlau) were included during the sol-gel route. The methylene blue dye was used as a pollutant model in the photodegradation reaction. Distilled water was used in all catalyst preparations.

Preparation of the photocatalysts. The TiO_2 nanoparticles were prepared using simple sol-gel "one-pot" method as follows. First, titanium(IV) isopropoxide was mixed with isopropyl alcohol under stirring at 30°C. Then ethyl acetoacetate (Eacac) was added as complexing agent with n(Eacac)/n(Ti) = 2 molar ratio. The mixture was kept under stirring at 30°C for 1 h. An appropriate amount of the dopant precursor (2% mol) was dissolved in an aqueous solution of nitric acid (0.1 mol L^{-1}). The solution was then added dropwise to the above mixture for insuring hydrolysis and condensation reactions. The stirring was continued until a translucent gel was formed (Fig. 1). The gel thus obtained (after about 6 min) was aged for 24 h, dried under supercritical conditions of the solvent (T = 245°C, P = 47.5 bar), ground to a fine powder and then calcined in a tubular furnace under pure oxygen flow of 30 cm^3/min and heating at a temperature rise of 2 deg/min up to 450°C for 4 h. Undoped TiO_2 was prepared following the same procedure as doped materials, without the addition of dopant precursors.

Characterization. The X-ray powder diffraction (XRD) patterns of each sample were recorded with an automated PHILIPS PANALYTICAL diffractometer equipped with a CuK_α radiation source (λ = 1.5405 Å) and operating at a voltage of 40 kV and a current of 30 mA. The angular range selected for recording is between 5° and 70° and the scanning speed is 2° min^{-1}. The diffractograms were processed using the X'Pert High Score Plus program. The crystallite size was estimated by the Scherrer equation:

$$D = \frac{k\lambda}{\beta \cos\theta},$$

where D is the average crystallite size (nm), k is the Scherrer constant (0.9), λ is the X-ray radiation wavelength (0.154 nm), β is the full width at half maximum of the selected peak and θ is the diffraction angle.

Measurements of specific surface areas as well as porosity were estimated according to the Brunauer–Emmett–Teller (BET) method using an automated MICROMERITICS device type ASAP 2020. Prior to

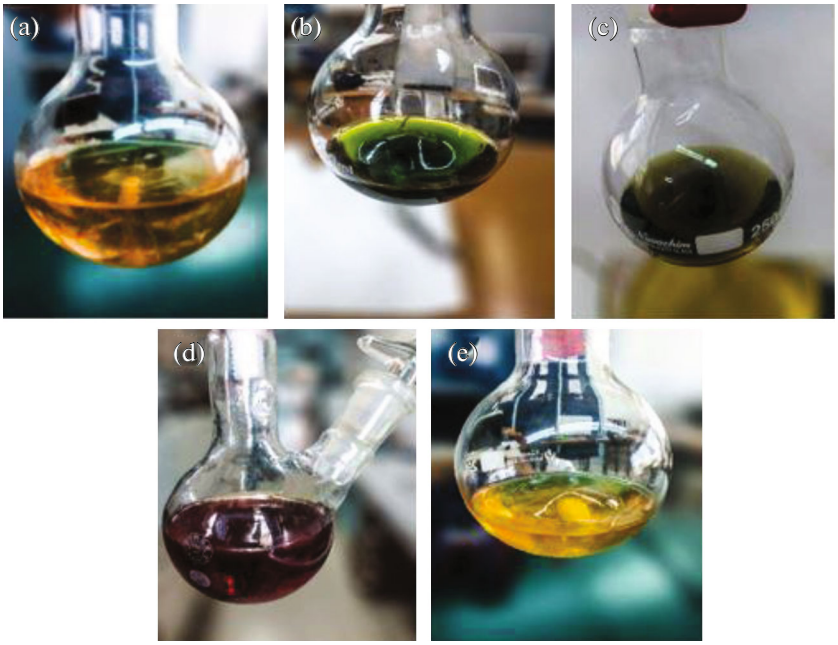

Fig. 1. Aspect of the gel of TiO_2 doped materials: (a) Pure TiO_2, (b) Cr–TiO_2, (c) Co–TiO_2, (d) Fe–TiO_2, and (e) Zr–TiO_2.

analysis, the samples were degassed under vacuum at 200°C for 5 h in order to remove away all adsorbed and absorbed molecules in the pores. The results are given automatically by the software installed on the instrument.

The UV-Visible absorption spectra were obtained using a Perkin-Elmer Lambda 45 spectrophotometer with an integrating sphere of RSA-EP-20 type allowing the measurement of the diffuse reflectance and controlled by a microcomputer which ensures the acquisition of the spectra and their mathematical processing. The spectra were recorded at room temperature between 200 and 800 nm.

The device used for photoluminescence spectroscopy (PL) consists of a pulsed laser whose emission wavelength can be changed. The laser allows measurements with an excitation ranging from 410 to 710 nm. The laser beam is guided to the sample by sets of mirrors. The emitted light then converges via lenses to a monochromator and then a photomultiplier and the output signal can then be analyzed via a computer.

Photocatalytic activity studies. Photocatalytic performances of the as-prepared catalysts were evaluated in the degradation reaction of methylene blue (MB) dye under solar irradiation. Photocatalytic experiments were carried out at room temperature and at neutral pH. Before starting the photocatalytic reaction, 50 mg of the catalyst powder was added to 100 ml of the methylene blue in aqueous solution (10 mg L^{-1}). The suspension was stirred in the dark for 30 min to reach the adsorption-desorption equilibrium conditions prior to irradiation [38]. The solution was then exposed to solar irradiation. The whole series of experiments was carried out simultaneously in order to be under the same reaction conditions of solar light intensity. After 1 h of irradiation, the samples were filtered and absorbance measurements were performed using a Hanon Instruments type I3 spectrophotometer at a wavelength of 665 nm which is the maximum absorption of methylene blue (λ_{max}). The percentage of photodegradation was calculated as follows:

$$\text{Photodegradation}\,(\%) = \left(\frac{A_0 - A}{A_0}\right) \times 100,$$

where A_0 and A are the absorbance of MB solution before and after irradiation, respectively.

RESULTS AND DISCUSSION

Characterization Results

The XRD diffractograms of pristine and doped TiO_2 samples are displayed in Fig. 2. XRD patterns show that all TiO_2 nanomaterials exhibit the similar pattern with only the characteristic peaks of the TiO_2 pure anatase phase. The main XRD diffraction peaks are assigned to the (101), (004), (200), (105), (211) and (204) crystal planes of anatase phase of TiO_2 (JCPDS card no. 21-1272). The diffraction peaks are intense and sharp highlighting a good crystallinity of the TiO_2 nanomaterials. Markedly, no other peaks related to doping metal phases are detected. This suggests that Cr^{3+}, Fe^{3+}, Co^{2+} and Zr^{4+} ions are either well incorporated into the TiO_2 lattice structure and/or well dispersed on the surface of TiO_2 catalyst. The TiO_2 cell parameters, the increase in cell volume (%)

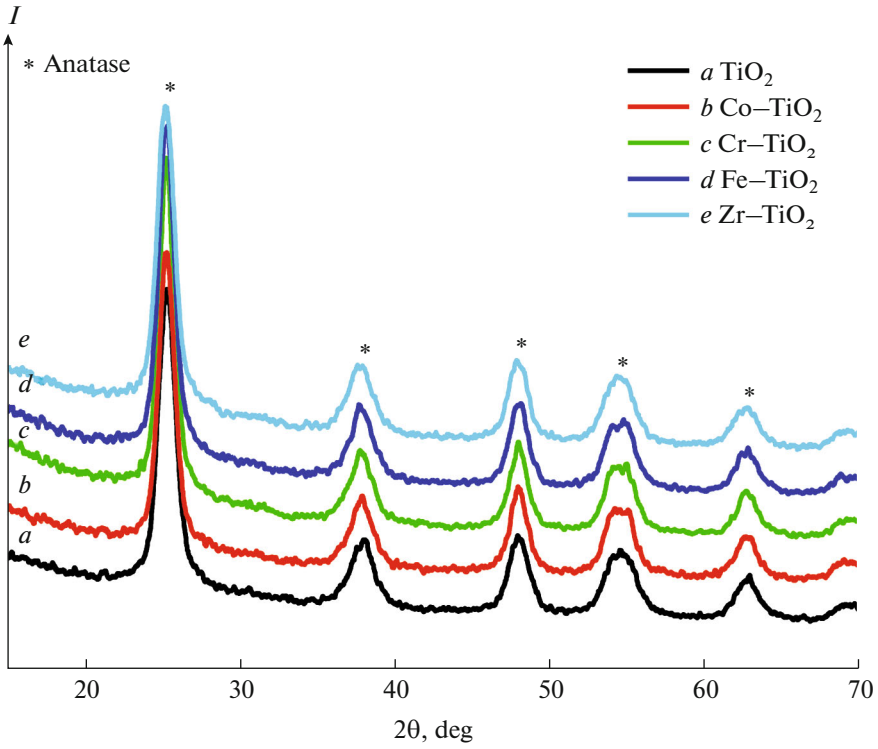

Fig. 2. XRD patterns of bare and metal-doped TiO_2 catalysts.

[39], and the ionic radii of dopant ions are given in Table 1. The results show a variation in cell parameters after insertion of the dopant ions, and thereafter an increase in TiO_2 cell volume. These findings may be attributed to the size of the dopant ions larger than that of Ti^{4+} [40]. The insertion of dopant ions could be accompanied by the introduction of oxygen vacancies to preserve electronic neutrality. For Cr^{3+}, Fe^{3+} and Co^{2+} doping, the creation of oxygen vacancies is possible since their lower valence than the host ion Ti^{4+}. However, for Zr^{4+} doping, the creation of oxygen vacancies is mainly attributed to the size of zirconium ion (86 pm) larger than that of the titanium host one (74.5 pm). According to Swetha et al. [41] the formation of complex defects with Zr atoms and an oxygen vacancy in close proximity is energetically more favorable and this for steric reasons. In Kröger and Vink notation, the probable chemical reaction can be represented in a favorable way.

$$ZrO_2 \rightarrow Zr'_{Ti} + V_{\ddot{O}} + O_o + 1/2O_2 + 2e^-,$$

where Zr'_{Ti} is the Zr ion at a Ti lattice site with a single charge deficiency, $V_{\ddot{O}}$ is a doubly ionized oxygen vacancy, O_o is an oxygen ion in the normal lattice site where the concentration of the intrinsic defect ($V_{\ddot{O}}$) becomes equal to the concentration of the extrinsic impurity [41].

Moreover, a variety of research works have reported the creation of oxygen vacancies through Zr-doped TiO_2 material [42–45].

Table 1. Cell parameters, Increase in cell volume, ionic radii of the dopant ions, crystallite size and gap energy of the TiO_2 catalysts

Materials	Cell parametrs		Increase in cell volume, %	Ionic radii, pm [40]	Crystallite size, nm	Gap energy, eV
	$a = b$, Å	c, Å				
TiO_2	3.7818	9.3193	0	74.5	7.9	3.28
$Cr–TiO_2$	3.7828	9.3789	0.693	75.5	14.2	2.77
$Fe–TiO_2$	3.7821	9.3996	0.882	78.5	9.5	3.15
$Co–TiO_2$	3.7824	9.3642	0.514	79.0	10.1	2.70
$Zr–TiO_2$	3.7850	9.4317	1.377	86.0	12.9	3.26

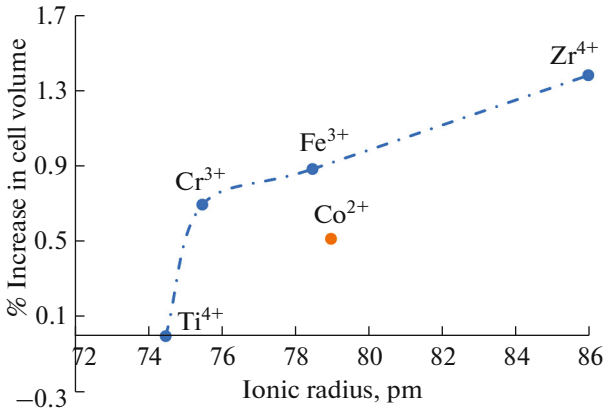

Fig. 3. Evolution of the cell volume variation after substitution compared to pristine TiO_2 anatase cell volume for the various doped catalysts.

Figure 3 shows the variation of the cell volume after doping compared to pristine TiO_2 as a function of the ionic radius of the dopants. It is clearly seen from Fig. 3 that the overall trend of the curve shows an increase in the cell volume of TiO_2 by increasing the ionic radius of the dopant ions compared to the cell volume of pristine oxide. However, cobalt escapes this trend which might be attributed to the presence of a part of the cobalt on the catalyst surface in addition to the substitution of Ti^{4+} cations in TiO_2 network [46]. Similar observations were reported by Wang et al. [47] where the authors revealed an increase in TiO_2 cell parameters accompanied by a shift in the diffraction angle for TiO_2 matrix doped with zirconium. Furthermore, the average crystallite size of TiO_2 nanomaterials is calculated using Scherrer's formula and the obtained values are given in Table 1. It can be seen that all the samples are characterized by a nanometric size and that the addition of dopants contributes to a crystal growth compared to pristine titanium oxide. Similar results have been reported in the literature [48] and attributed to the size of dopant ions according to Liu et al. [49]. As is clear, the average crystallite size values can explain the presence of the anatase phase according to the literature [50] which indicates that this phase is stable for an optimal particle size below 14 nm.

In order to get inside the structure of the as-prepared pure TiO_2 nanomaterials, high resolution TEM measurement was conducted and the results are presented in Fig. 4. As can be seen, the pure TiO_2 particles are morphologically well-dispersed and highly ordered, and most of the particles are of spherical shape. The average particle size turns out to be 6–8 nm highlighting a quantum-sized TiO_2 particles. The average particles size obtained from the high-resolution TEM micrograph matches well with that obtained by XRD analysis which may also confirm the nanometric size of all the doped TiO_2 catalysts. It is worthy to point out that, the preparation method used in the present work, rarely used in literature, is ideally suited to synthesize quantum sized TiO_2 materials efficient in various applications.

Textural properties were evaluated by N_2 adsorption-desorption analysis at 77 K. The evolution of textural properties of pristine and doped TiO_2 catalysts is detailed in Fig. 5. According to the obtained results, it is clearly seen that doping does not significantly affect the textural properties and that TiO_2 catalysts conserve after doping, high surface areas ranging from 173 to 197 $m^2\ g^{-1}$ and relatively high pore volumes. The high surface areas obtained is mainly related to the process of solvent evacuation during the drying of gels. In fact, the simple evaporation in an oven is not controlled, thereby a liquid-vapour interface is created inside the

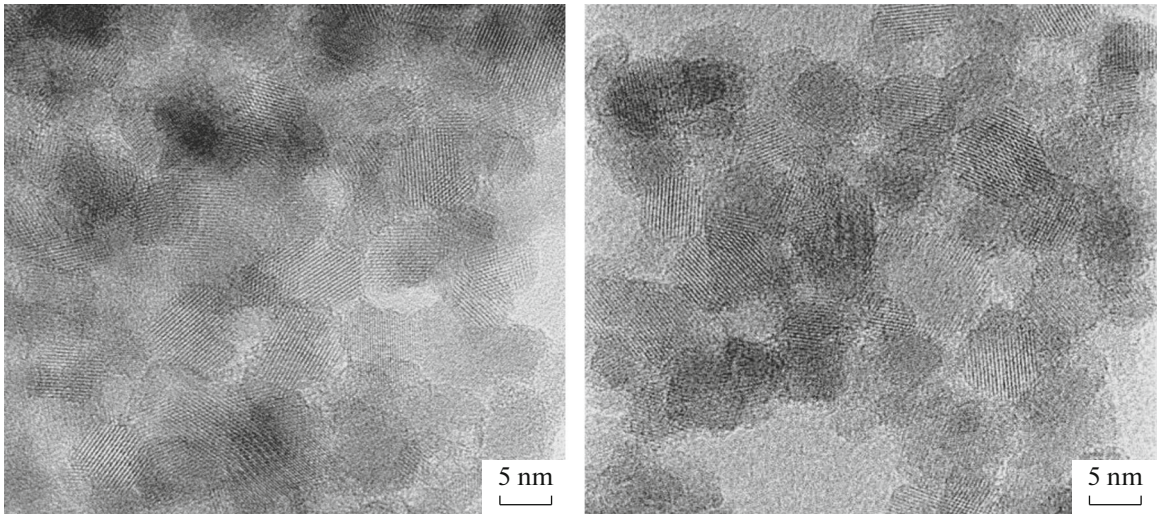

Fig. 4. High resolution TEM image of pure TiO_2 catalyst.

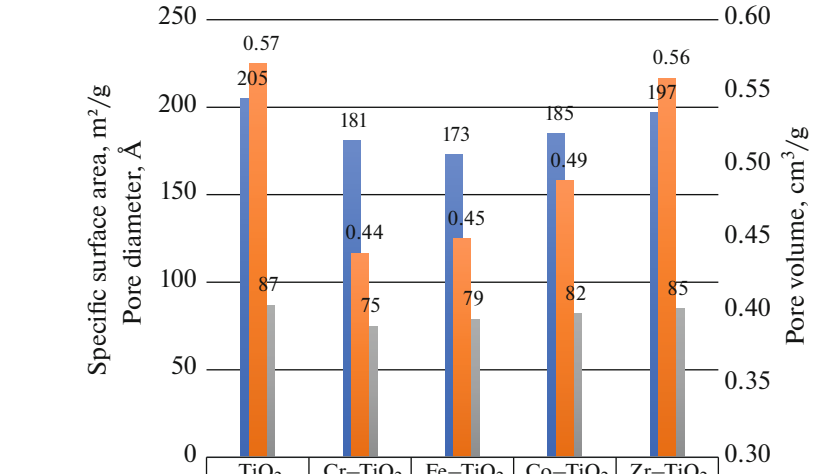

	TiO_2	Cr–TiO_2	Fe–TiO_2	Co–TiO_2	Zr–TiO_2
Specific surface area	205	181	173	185	197
Pore diameter	87	75	79	82	85
Pore volume	0.57	0.44	0.45	0.49	0.56

Fig. 5. Evolution of TiO_2 textural properties of pristine and metal-doped TiO_2.

gel pores which can create a surface tension resulting in a shrinkage of the pores of the xerogel solid and then a decrease in specific surface area. However, when the solvent is removed under its supercritical conditions, which is the case in this work, the evaporation is controlled thus the liquid–vapour interface and the shrinkage phenomenon are prevented, which leads to an aerogel solid characterized by a large porosity and a low density. Interestingly, the aerogels abtained in this work, are characterized by surface areas considerably higher than xerogels reported in literature [51–53]. Nevertheless, a slight decrease of the surface area and pore volume and diameter of metal-doped TiO_2 compared to the pristine material is observed. This finding might be attributed to the increase of the crystallite size of titanium dioxide after its modification and to the partial obstruction of some pores of catalysts by dopant species. These results seem to be in good agreement with the work of Romero [54] on iron-doped TiO_2 and Hamadanian et al. [35] in the case of cobalt-doped TiO_2 catalyst, where the authors explain the reduction in surface area by the agglomeration of particles due to the dopant. Based on N_2 physisorption analysis results, it can be concluded that doping seems to have the effect of promoting the creation of larger particles by the agglomeration of smaller ones and thus reducing the porosity of the matrix.

The N_2 adsorption–desorption isotherms of TiO_2 samples are shown in Fig. 6a. According to IUPAC classification [55], the as-prepared catalysts exhibited a type IV(a) isotherm characteristic of mesoporous solids with a uniform and structured surface. Furthermore, all samples exhibit H2(b) type hysteresis loops, typical of sample with narrow ink-bottle type interconnections. H2 type hysteresis loops are given by complex pore structures in which network effects are important. Particularly, the H2(b) type hysteresis loop is characterized by a much larger pore size distribution. This type of loops and the monomodal and wide porous distribution shown in Fig. 6b, might prove that our materials are derived from the agglomeration of particles of relatively similar sizes but with pores of ill-defined sizes and distributions [55].

In order to investigate the effect of doping on optical response of TiO_2-based nanostructures, a series of UV-Vis diffuse reflectance measurements were performed in the range 200–800 nm and the results are given in Fig. 7. It is clearly seen that bare and doped TiO_2 samples show a strong absorption in the UV region. The spectra of photocatalysts show that the absorption of metal-doped TiO_2 into visible region depends to a large extent on the dopant nature. A marked shift towards higher wavelengths is observed for Cr, Fe and Co doped TiO_2 samples compared to the pristine oxide. This finding obviously reveals a modification in electronic band structure of TiO_2. Actually, the shift of absorption towards the visible region suggests probably the creation of intermediate energy levels between conduction and valence bands and thus a decrease in gap energy. The red shift is more pronounced for samples doped with cobalt and chromium, which might be attributed to the presence of Ti–O–M bonds and the incorporation of dopants in the TiO_2 matrix. However, no significant shift towards the visible region is observed for Zr doped-TiO_2 catalyst, suggesting that zirconium doping does not modify the electronic structure of TiO_2.

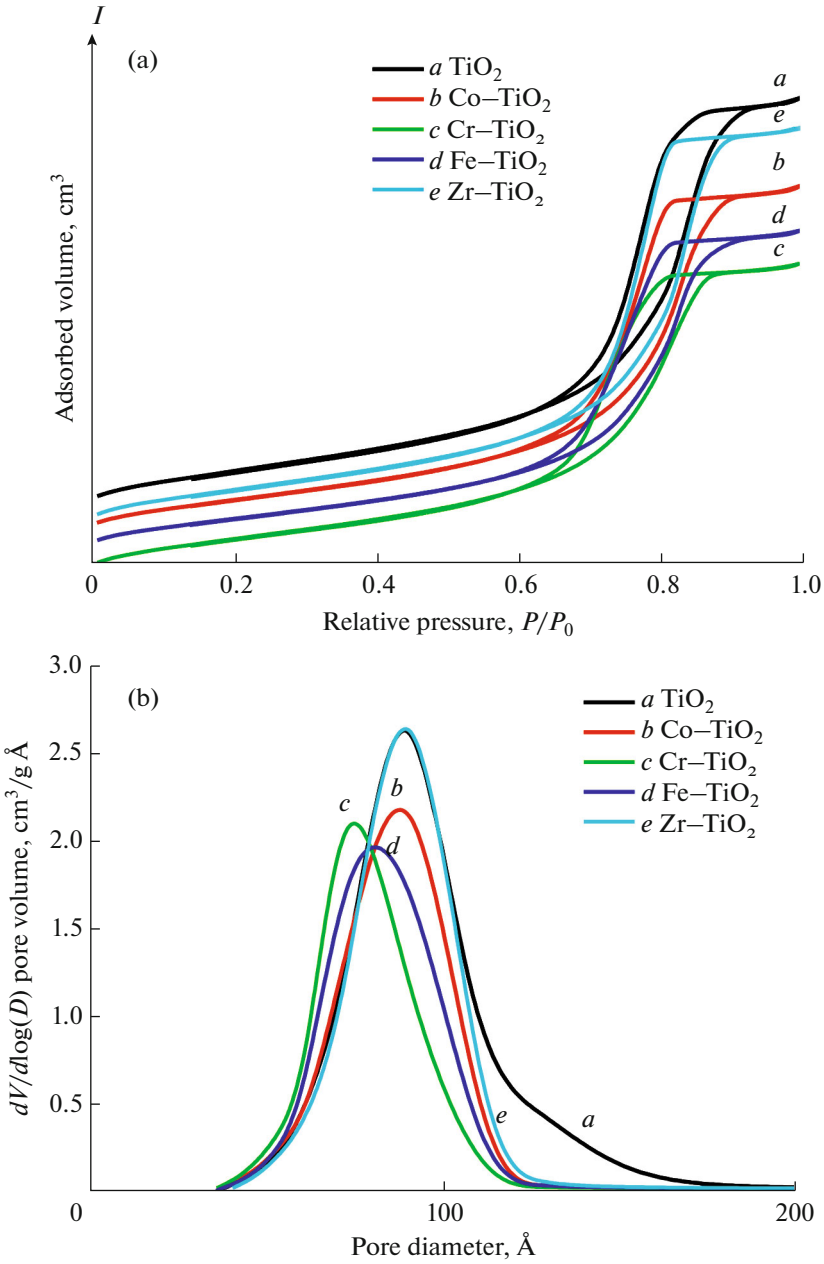

Fig. 6. (a) N_2 adsorption–desorption isotherms and (b) BJH pore size distribution of pristine and metal-doped TiO_2 photocatalysts.

The band gap energies of the materials are determined from Tauc plot method and presented in Fig. 8 and Table 1. The results show that doping decreases the gap energy of TiO_2 for the materials containing Cr, Co and Fe as dopants, which could be related to the involvement of new energy levels in the band gap, as previously reported [56, 57]. For metals such as chromium and iron, the energy intensity of the *d* electrons is lower than that of the 3*d* orbit of TiO_2 and lies between the conduction and valence bands of the semi-conductor. Therefore, their addition could lower the conduction band and reduce the gap energy of TiO_2 [58]. On the other hand, zirconium doping does not significantly modify the gap energy of TiO_2 which is in good agreement with the works of Wang et al. [59] and D'yachkov et al. [60].

Based on the color of the powder samples, it was noticed that the Cr, Co and Fe doped TiO_2 are colored while the color of Zr-doped TiO_2 powder did not change and remains white. Therefore, pure and Zr-doped TiO_2 do not absorb in the visible light region.

It is well known that surface defects as well as an effective charge separation are quite crucial in the

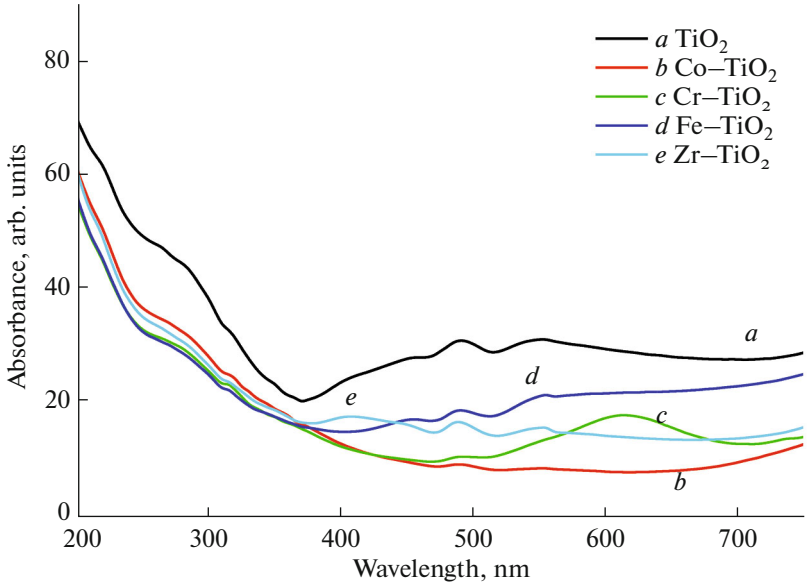

Fig. 7. UV-visible reflectance diffuse spectra of TiO_2 catalysts.

photocatalytic processes. Such results could be evidenced by photoluminescence spectroscopy (PL). PL spectra of the as-prepared samples are displayed in Fig. 9. It is found that the spectra of all samples showed emission peaks at 405, 421, 446 and 486 nm and a broad peak centered at 520 nm. Following previous reports in the literature, emission peaks shown at 405, 421 and 446 nm are probably attributed to the recombination of excited electrons–holes inside the bulk lattice of TiO_2 [61, 62]. The emission band at 486 nm is observed owing to the charge transfer from Ti^{3+} to oxygen anion in TiO_6^{2-} octahedral complex associated with oxygen vacancies [63]. The peak at ~520 nm can be attributed to the recombination of the surface oxygen vacancies with trapped electrons [64]. It was observed that doping leads to a decrease of the emission bands intensity, in particular emission bands related to the recombination of photogenerated e^-/h^+ suggesting a decrease in recombination rate of photogenerated e^-/h^+ compared to undoped oxide. These results are in good agreement with the work of Jaimy et al. [65]. Nevertheless, the decrease observed in the intensity of emission bands originated from recombination with oxygen vacancies may negatively affect the performance of the catalysts in photocatalysis. However, in the case of zirconium doping, the intensity of the band around 520 nm increases compared to that of all other samples, which might enhance the catalyst performance compared even to pristine oxide [66]. Indeed, the insertion of zirconium leads to the largest increase in cell volume as observed by XRD analysis and then a cell distortion which favors the creation of high amount of oxygen defects. This finding is particularly related to the size of Zr^{4+} (86 nm) larger than that of titanium Ti^{4+} (74.5 nm). Similar results have been obtained in the literature where authors have reported the creation of oxygen vacancies through Zr-doped TiO_2 material [42–45].

Therefore, PL results show that the role of zirconium consists mainly in generating surface oxygen vacancies able to trap photogenerated electrons thus providing a charge separation that can enhance photoactivity. Zirconium also limits the bulk recombination rate compared to bare TiO_2 oxide, which is related to the creation of surface defects.

Photocatalytic Studies

Blank test. A blank test was performed without catalyst to evaluate the reactivity of methylene blue under photocatalytic reaction conditions. After 1 h of solar irradiation, the results obtained showed that the degradation of MB is exceedingly slow without photocatalyst under visible light and ambient temperature since the percentage of photodegradation does not exceed 9%. It can be concluded that the photodegradation of dyes requires the introduction of a catalyst into the reaction medium.

Effect of doping on the photocatalytic properties of TiO_2 nanostructures in the degradation reaction of MB. The collected results of MB photodegradation are shown in Fig. 10. It is clearly seen that all doped TiO_2 catalysts are active in MB photodegradation and that the nature of the dopant affects activity. According to the experimental studies, the effectiveness of doped titanium dioxide is not correlated to the value of gap energy. In fact, the catalyst zirconium doped TiO_2 exhibits the highest photocatalytic efficiency, although its gap energy was not reduced compared to pure and doped TiO_2. Consequently, the optical properties are not the main factor affecting the photocatalytic degradation of MB.

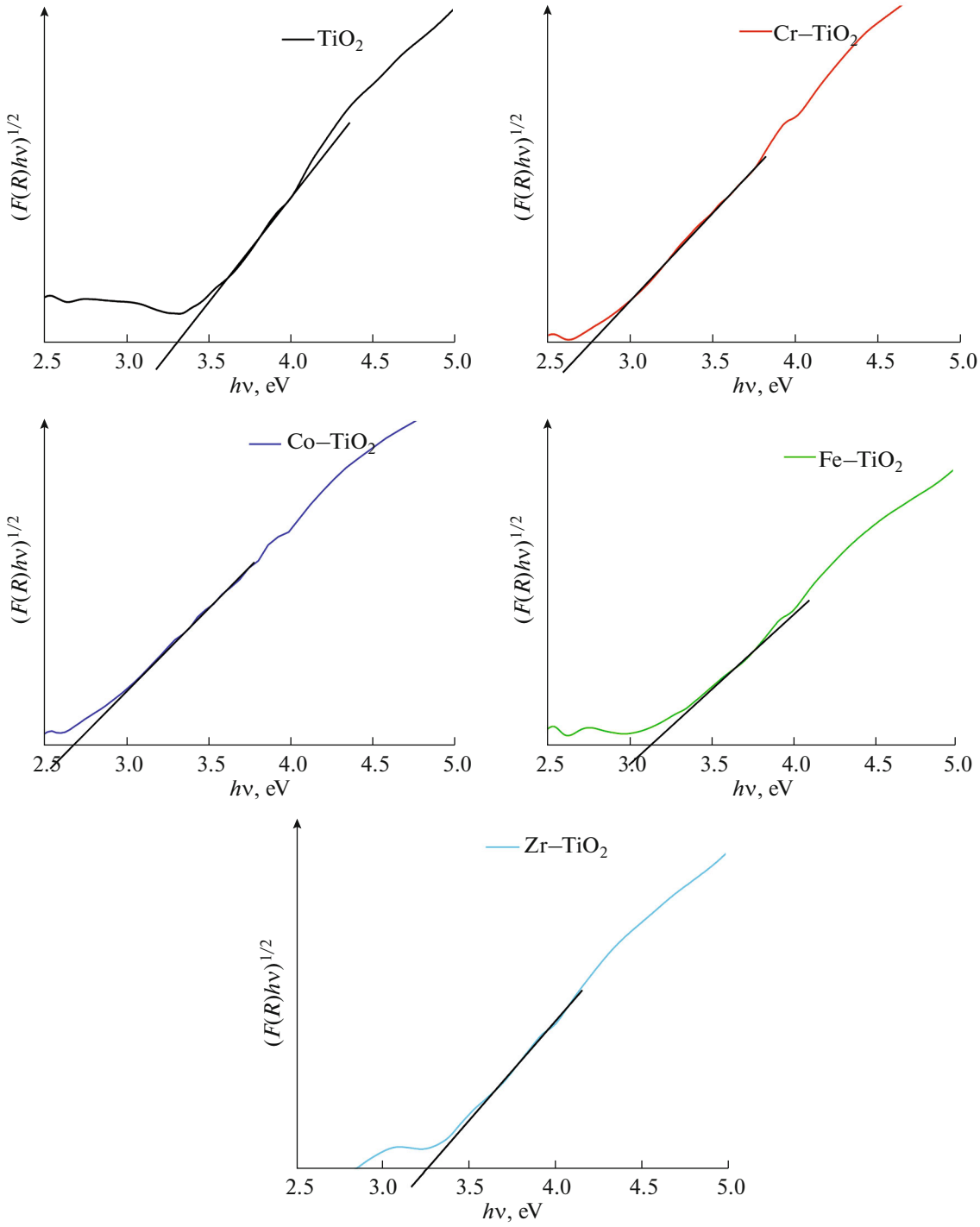

Fig. 8. Tauc plots for band gap estimations of pure and doped TiO_2 catalysts.

The improvement of the photocatalytic activity of Zr–TiO_2 compared to doped TiO_2 catalysts could be correlated to its textural properties. Indeed, it has been shown by nitrogen physisorption at 77 K that zirconium doped TiO_2 catalyst has the largest specific surface area (197 m^2/g) and the best porosity compared to other doped catalysts. A relatively high surface area could increase the available active sites surface, and consequently leads to a higher charge separation rate for photocatalysis.

The study of optical properties show that doping decreases the gap energy and shifts the absorption to the visible region for Cr, Co and Fe doped TiO_2. However, although the optical properties of these catalysts are better than those of undoped TiO_2, the reduction of oxygen defects seems to significantly affect their

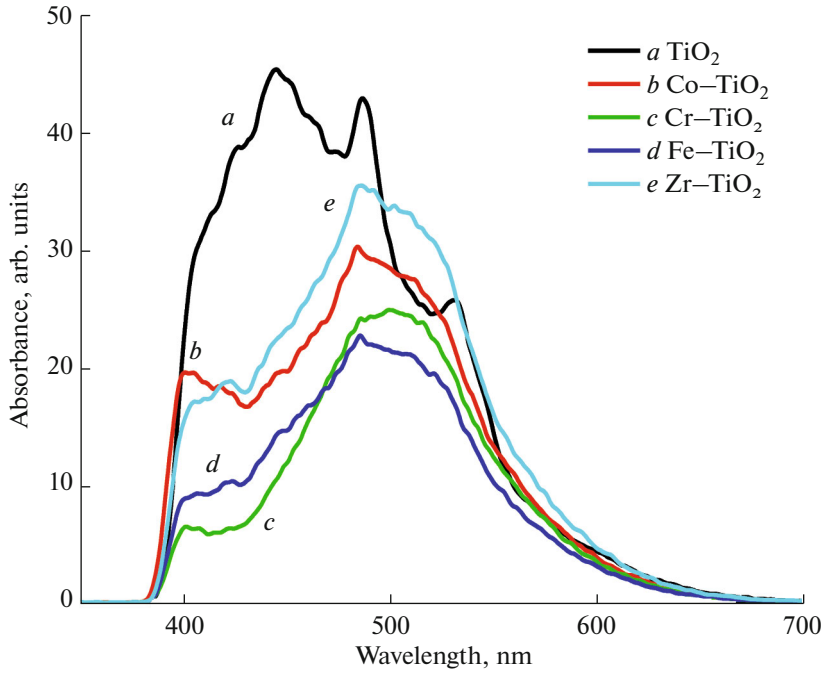

Fig. 9. Photoluminescence spectra of the TiO_2 photocatalysts.

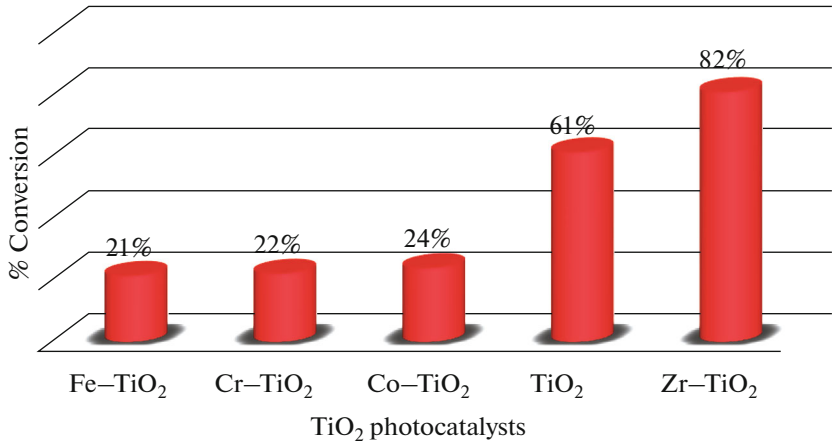

Fig. 10. Photodegradation conversion of MB over undoped and doped TiO_2 nanomaterials.

photocatalytic efficiency. However, the higher photoactivity of zirconium doped TiO_2 compared to pure oxide, may be attributed to a combination of a lower recombination rate of photogenerated e^-/h^+ and mainly a higher concentration of oxygen defects given its higher size and same charge than that of Ti^{4+}. The increase in cell volume, in the case of zirconium doped TiO_2, seems to have a positive effect on photocatalytic activity.

Therefore, the photocatalytic efficiency in our case, cannot be explained by optical properties. A reduction in gap energy does not seem to improve photocatalytic activity as shown in the case of chromium, cobalt and iron doping. On the other hand, zirconium doping shows the highest catalytic efficiency even if it doesn't improve the optical properties of TiO_2. Thus, it is worthy to point out that photocatalytic efficiency is significantly affected by the density of oxygen defects; an increase in the concentration of oxygen defects, in addition to favorable charge separation and textural properties, improves photoactivity as shown in the case of zirconium doped TiO_2. Actually, the photogenerated electrons will be able to be captured by these oxygen vacancies producing strong oxidizing species like $OH^{\bullet}$ or $O_2^{\bullet-}$ enhancing in fine the photocatalytic activity. Our findings leads to conclude that the increase or reduction of oxygen defects den-

sity seems to be a key parameter of photocatalytic efficiency.

Interestingly, the efficiency of as-prepared zirconium doped TiO_2 catalyst has been compared with existing compounds. The photocatalytic activity achieved in this work is found to be substantially higher than that reported in previous works [67, 68]. It is worthy to point out that, the preparation method used in the present work, hardly used in the literature, allows the preparation of nano-sized and even quantum-sized materials with an efficient particle distribution and ordering, high surface areas and an extended absorption towards visible region. This could reveal promising materials useful in several potential applications. Therefore, it seems interesting to find the optimal amount or precursor of chromium, iron and cobalt dopant to obtain the highest photocatalytic efficiency. In this context, Wang et al. [37] reported for the iron-doped catalyst that the highest catalytic activity was achieved with 1% iron. However, a very small amount of iron (0.05%) seems detrimental to the photocatalytic decomposition of methyl orange.

Suggested photocatalytic mechanism. It is generally acknowledged that heterogeneous photocatalysis on TiO_2 involves four processes; charge-carrier generation, charge-carrier recombination, charge-carrier trapping, and photocatalytic reactions. Present experimental results evidence the formation of intermediate energy levels within the band gap of TiO_2 following doping with Cr, Co and Fe. This is probably resulting from the injection of electrons from TiO_2 to the dopant *d* level. Nevertheless, a significant decrease in photoactivity is observed for these catalysts. This suggests that the intermediate levels in the band gap are more likely to behave as e^-/h^+ recombination centers than as trap sites, thus preventing the production of free radicals responsible for the degradation of pollutants. In the case of zirconium doping, the results highlighted a significant enhancement of photocatalytic properties of titania material. The incorporation of Zr^{4+} in TiO_2 matrix, did not lead to the formation of intermediate levels in its band gap, and generates surface oxygen vacancies due to its larger ionic radius and same charge than Ti^{4+}. The surface oxygen vacancies can participate in the capture of photogenerated electrons thus increasing the charge carriers lifetime. This helps to maintain a high photocatalytic activity. Subsequently, the reduction of oxygen by injected electrons allows the formation of superoxide anion radicals ($O_2^{\bullet -}$), which in turn react with H_2O molecules to form hydroperoxyl radicals ($HOO^{\bullet}$) and hydroxyl ions (OH^-). While, the hydroxyl radicals ($OH^{\bullet}$) were generated by the reaction of positive holes with electron donors such as H_2O and OH^- anions adsorbed on the surface of the semi-conductor. The powerful species ($OH^{\bullet}$ and $O_2^{\bullet -}$) will participate in the degradation of the pollutants adsorbed on the surface of the catalyst.

This proposed mechanism of the photocatalytic decomposition of methylene blue is summarized in Scheme 1.

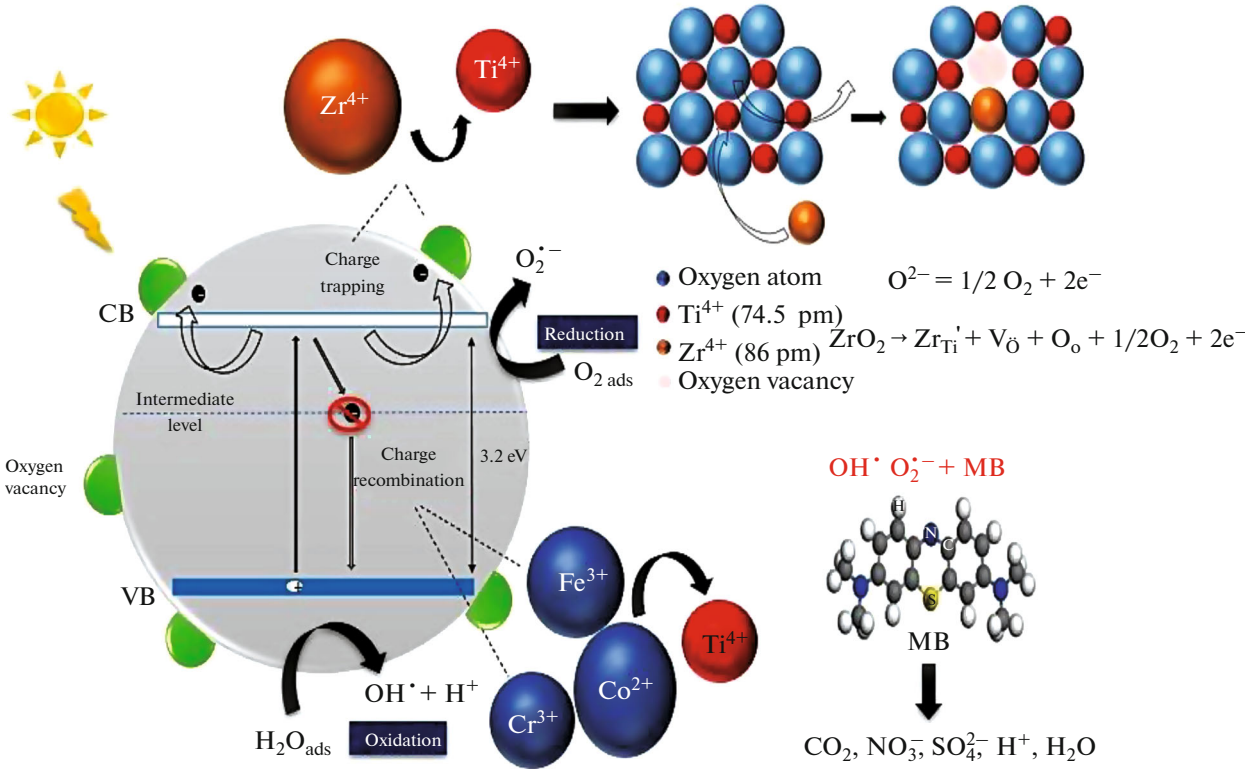

Scheme 1. Proposed photocatalytic mechanism of methylene blue degradation.

CONCLUSIONS

A comparative study of the effect of chromium, iron, cobalt and zirconium doping on the structural, textural, optical and photocatalytic properties of TiO_2 nanomaterials prepared by the sol-gel "one-pot" route is presented in this work. It was revealed that the addition of zirconium with higher size than Ti^{4+} improved the photocatalytic features compared to undoped and doped TiO_2 catalysts. TEM analysis of pristine oxide revealed quantum-sized, well-dispersed and highly ordered particles. All the catalysts showed the presence of the anatase phase and high surface areas. In addition, an increase in cell volume was demonstrated by increasing the size (ionic radius) of the dopant ion. Optical characterizations indicated that doping with Cr, Co and Fe reduced the gap energy and thus significantly shifted the absorption to the visible region. However, Zr doping did not modify the eletronic structure of TiO_2. Photoluminescence analysis showed that doping reduces the amount of oxygen vacancies which might reduce photocatalytic activity. An exception was made for zirconium doping which increases the oxygen defects, thus can improve its photocatalytic activity. Interestingly, Zr^{4+} having a larger size and same charge than Ti^{4+} causes a cell distortion as can be seen by XRD analysis, thus allowing the creation of a large amount of oxygen vacancies and enhances the photocatalytic activity. Despite the improvement of optical properties, a limited photoactivity is found for the other catalysts which was mainly attributed to the intermediate levels acting as recombination centers and the low amount of oxygen vacancies. According to the mechanism, the overall catalytic efficiency is determined by two critical processes. These are the competition between charge recombination, and charge trapping ensuring a charge separation which is provided in the present work by oxygen defects. The increase in the lifetime of charge carriers is expected to result in higher catalytic efficiencies for photocatalysis.

FUNDING

The authors would like to thank the Tunisian Ministry of Higher Education and Scientific Research for financial support.

CONFLICT OF INTEREST

The authors declare that there is no conflicts of interest regarding the publication of this article.

REFERENCES

1. P. Chowdhary, A. Raj, and R. N. Bharagava, Chemosphere **194**, 229 (2018). https://doi.org/10.1016/j.chemosphere.2017.11.163
2. H. I. Abdel-Shafy and M. S. M. Mansour, Egypt. J. Petrol. **25**, 107 (2016). https://doi.org/10.1016/j.ejpe.2015.03.011
3. M. Amde, J. F. Liu, and L. Pang, Environ. Sci. Technol. **49**, 12611 (2015). https://doi.org/10.1021/acs.est.5b03123
4. H. B. Quesada, A. T. A. Baptista, L. F. Cusioli, et al., Chemosphere **222**, 766 (2019). https://doi.org/10.1016/j.chemosphere.2019.02.009
5. C. Santhosh, V. Velmurugan, G. Jacob, et al., Chem. Eng. J. **306**, 1116 (2016). https://doi.org/10.1016/j.cej.2016.08.053
6. N. Divya, A. Bansal, and A. K. Jana, Mater. Sci. Forum **734**, 349 (2013). https://doi.org/10.4028/www.scientific.net/MSF.734.349
7. D. B. Miklos, C. Remy, M. Jekel, et al., Water Res. **139**, 118 (2018). https://doi.org/10.1016/j.watres.2018.03.042
8. R. Fagan, D. E. McCormack, D. D. Dionysiou, and S. C. Pillai, Mater. Sci. Semicond. Process. **42**, 2 (2016). https://doi.org/10.1016/j.mssp.2015.07.052
9. A. J. Haider, Z. N. Jameel, and I. H. M. Al-Hussaini, Energy Procedia **157**, 17 (2019). https://doi.org/10.1016/j.egypro.2018.11.159
10. J. Cai, J. Shen, X. Zhang, Y. H. Ng, et al., Small Methods **3**, 1800184 (2019). https://doi.org/10.1002/smtd.201800184
11. S. Ghosh and A. P. Das, Toxicol. Environ. Chem. **97**, 491 (2015). https://doi.org/10.1080/02772248.2015.1052204
12. N. Rahimi, R. A. Pax, and E. M. Gray, Prog. Solid State Chem. **44**, 86 (2016). https://doi.org/10.1016/j.progsolidstchem.2016.07.002
13. J. Tian, Z. Zhao, A. Kumar, et al., Chem. Soc. Rev. **43**, 6920 (2014). https://doi.org/10.1039/C4CS00180J
14. V. Kumaravel, S. Mathew, J. Bartlett, and S. C. Pillai, Appl. Catal. B **244**, 1021 (2019). https://doi.org/10.1016/j.apcatb.2018.11.080
15. A. A. Sadovnikov, E. G. Nechaev, A. N. Beltiukov, et al., Russ. J. Inorg. Chem. **66**, 460 (2021). https://doi.org/10.1134/S0036023621040197
16. R. Daghrir, P. Drogui, and D. Robert, Ind. Eng. Chem. Res. **52**, 3581 (2013). https://doi.org/10.1021/ie303468t
17. P. Mazierski, A. Mikolajczyk, B. Bajorowicz, et al., Appl. Catal. B **233**, 301 (2018). https://doi.org/10.1016/j.apcatb.2018.04.019
18. B. A. Bhanvase, T. P. Shende, and S. H. Sonawane, Environ. Technol. Rev. **6**, 1 (2017). https://doi.org/10.1080/21622515.2016.1264489
19. R. Xie, D. Lei, Y. Zhan, B et al., Chem. Eng. J. **386**, 121025 (2020). https://doi.org/10.1016/j.cej.2019.02.112
20. O. A. Shilova, G. G. Panova, S. V. Mjakin, et al., Russ. J. Inorg. Chem. **66**, 765 (2021). https://doi.org/10.1134/S0036023621050181
21. N. Liu, X. Chen, J. Zhang, and J. W. Schwank, Catal. Today **225**, 34 (2013). https://doi.org/10.1016/j.cattod.2013.10.090

22. Y. Li, W. Zhang, X. Shen, et al., Chin. J. Catal. **36**, 2229 (2015). https://doi.org/10.1016/S1872-2067(15)60991-3
23. K. Choi, S. H. Lee, J. Y. Park, et al., Mater. Lett. **112**, 113 (2013). https://doi.org/10.1016/j.matlet.2013.08.101
24. A. S. Mokrushin, N. P. Simonenko, T. L. Simonenko, et al., Russ. J. Inorg. Chem. **66**, 1425 (2021). https://doi.org/10.1134/S0036023621090060
25. C. J. Brinker, A. J. Hurd, P. R. Schunk, et al., J Non-Cryst. Solids **147**, 424 (1992). https://doi.org/10.1016/S0022-3093(05)80653-2
26. A. B. Albadarin, M. N. Collins, M. Naushad, et al., Chem. Eng. J. **307**, 264 (2017). https://doi.org/10.1016/j.cej.2016.08.089
27. L. Mouni, L. Belkhiri, J. C. Bollinger, et al., Appl. Clay Sci. **153**, 38 (2018). https://doi.org/10.1016/j.clay.2017.11.034
28. A. V. Zdravkov, Yu. S. Kudryashova, and R. Sh. Abiev, Russ. J. Gen. Chem. **90**, 1677 (2020). https://doi.org/10.1134/S1070363220090145
29. Yu. S. Kudryashova, A. V. Zdravkov, V. L. Ugolkov, and R. Sh. Abiev, Glass Phys. Chem. **46**, 335 (2020). https://doi.org/10.1134/S1087659620040082
30. S. J. Alyani, A. E. Pirbazari, F. E. Khalilsaraei, N. A. Kolur, and N. Gilani, J. Alloys Compd. **799**, 169 (2019). https://doi.org/10.1016/j.jallcom.2019.05.175
31. H. H. Nguyen, G. Gyawali, A. Martinez-Oviedo, et al., J. Photochem. Photobiol. A **397**, 112514 (2020). https://doi.org/10.1016/j.jphotochem.2020.112514
32. M. J. Valero-Romero, J. G. Santaclara, L. Oar-Arteta, et al., Chem Eng J. **360**, 75 (2019). https://doi.org/10.1016/j.cej.2018.11.132
33. B. Duan, Y. Zhou, C. Huang, et al., Ind. Eng. Chem. Res. **57**, 14044 (2018). https://doi.org/10.1021/acs.iecr.8b03016
34. X. Fan, X. Chen, S. Zhu, et al., J. Mol. Catal. A Chem. **284**, 155 (2008). https://doi.org/10.1016/j.molcata.2008.01.005
35. M. Hamadanian, A. Reisi-Vanani, and A. Majedi, J. Iran. Chem. Soc. **7**, 52 (2010). https://doi.org/10.1007/BF03246184
36. Z. Li, W. Shen, W. He, and X. Zu, J. Hazard. Mater. **155**, 590 (2008). https://doi.org/10.1016/j.jhazmat.2007.11.095
37. X. H. Wang, J. G. Li, H. Kamiyama, Y. Moriyoshi, and T. Ishigaki, J. Phys. Chem. B **110**, 6804 (2006). https://doi.org/10.1021/jp060082z
38. H. Lachheb, E. Puzenata, A. Houas, et al., Appl. Catal. B **31**, 145 (2001). https://doi.org/10.1016/S0926-3373(00)00276-9
39. S. J. Sharmila, S. Ramalingom, C. Ravidhas, and A. M. E. Raj, J. Appl. Phys. **9**, 32 (2017).
40. R. D. Shannon, Acta Cryst. **32**, 751 (1976). https://doi.org/10.1107/S0567739476001551
41. S. Swetha, and R. G. Balakrishna, Chin. J. Catal. **32**, 789 (2011). https://doi.org/10.1016/S1872-2067(10)60200-8
42. D. Guerrero-Araque, D. Ramírez Ortega, P. Acevedo Peña, et al., J. Photochem. Photobiol. **335**, 276 (2017). http://dx.doi.org/doi:10.1016/j.jphotochem.2016.11.030
43. J. Lang, L. Matějová, Z. Matěj, et al., J. Solgel Sci. Technol. **90**, 369 (2019). https://doi.org/10.1007/s10971-019-04956-x
44. I. Singh, R. Kumar, and B. I. Birajdar, J. Environ. Chem. Eng. **5**, 2955 (2017). http://dx.doi.org/doi:10.1016/j.jece.2017.05.046
45. N. Yaacob, G. P. Sean, N. A. M. Nazri, **et al.**, J. Water Process. Eng. **39**, 101644 (2021). https://doi.org/10.1016/j.jwpe.2020.101644
46. Q. Chen, F. Ji, Q. Guo, et al., Res. J. Environ. Sci. **26**, 2440 (2014). https://doi.org/10.1016/j.jes.2014.03.003
47. J. Wang, Y. Yu, S. Li, L. Guo, et al., J. Phys. Chem. C **117**, 27120 (2013). https://doi.org/10.1021/jp407662d
48. S. Mugundan, B. Rajamannan, G. Viruthagiri, et al., Appl Nanosci. **5**, 449 (2014). https://doi.org/10.1007/s13204-014-0337-y
49. X. Liu, X. He, and Y. Fu, Acta Chim Sinica **66**, 1725 (2008).
50. J. Liqiang, S. Xiaojun, X. Baifu, et al., J. Solid State Chem. **177**, 3375 (2004). https://doi.org/10.1016/j.jssc.2004.05.064
51. J. Carbajo, A. Bahamonde, and M. Faraldos, Mol. Catal. **434**, 167 (2017). https://doi.org/10.1016/j.mcat.2017.03.018
52. C. Bogatu, D. Perniu, C. Sau, et al., Ceram. Int. **43**, 7963 (2017). https://doi.org/10.1016/j.ceramint.2017.03.054
53. J. Liang, J. Wang, K. Song, X. Wang, K. Yu, and C. Liang, J. Rare Earths. **38**, 148 (2020). https://doi.org/10.1016/j.jre.2019.07.008
54. A. M. J. Romero, *Nanoparticules à Base d'Oxyde de Titane pour la Photocatalyse* (Université Paris Sud, Paris XI, 2013). https://tel.archives-ouvertes.fr/tel-00868611/document
55. M. Thommes, K. Kaneko, A. V. Neimark, J. P. Olivier, F. Rodriguez-Reinoso, J. Rouquerol, and K. S. W. Sing, Pure Appl. Chem. **87**, 9 (2015). https://doi.org/10.1515/pac-2014-1117
56. O. G. Ellert, S. A. Nikolaev, D. A. Maslov, et al., Russ. J. Inorg. Chem. **63**, 1403 (2018). https://doi.org/10.1134/S0036023618110049
57. E. P. D'yachkov, D. V. Makaev, L. O. Khoroshavin, and P. N. D'yachkov, Russ. J. Inorg. Chem. **62**, 931 (2017). https://doi.org/10.1134/S0036023617070051
58. T. Kaur, A. Sraw, R. K. Wanchoo, and A. P. Toor, Mater. Today: Proc. **3**, 354 (2016). https://doi.org/10.1016/j.matpr.2016.01.020
59. Y. Wang, R. Zhang, J. Li, L. Li, and S. Lin, Nanoscale Res. Lett. **9**, 46 (2014). https://doi.org/10.1186/1556-276X-9-46
60. E. P. D'yachkov, I. A. Bochkov, V. A. Zaluev, and P. N. D'yachkov, Russ. J. Inorg. Chem. **62**, 1048 (2017). https://doi.org/10.1134/S003602361708006X

61. F. J. Knorr, C. C. Mercado, and J. L. McHale, J. Phys. Chem. C **112**, 12786 (2008). https://doi.org/10.1021/jp8039934

62. P. Sun, L. Liu, S. C. Cui, and J. G. Liu, Catal. Lett. **144**, 2107 (2014). https://doi.org/10.1007/s10562-014-1377-3

63. J. Liu, J. Li, A. Sedhain, J. Lin, and H. Jiang, J Phys Chem C. **112**, 17127 (2008). https://doi.org/10.1021/jp8060653

64. M. Hamandi, G. Berhault, F. Dappozze, et al., Appl. Surf. Sci. **412**, 306 (2017). https://doi.org/10.1016/j.apsusc.2017.03.261

65. K. B. Jaimy, S. Ghosh, S. Sankar, and K. G. K Warrier, Mater. Res. Bull. **46**, 914 (2011). https://doi.org/10.1016/j.materresbull.2011.02.030

66. J. Liqiang, Q. Yichun, W. Baiqi, et al., Sol. Energy Mater. Sol. Cells **90**, 1773 (2006). https://doi.org/10.1016/j.solmat.2005.11.007

67. S. N. R. Inturi, T. Boningari, M. Suidan, and P. G. Smirniotis, Appl. Catal. B **144**, 333 (2014). https://doi.org/10.1016/j.apcatb.2013.07.032

68. J. C. Colmenares, M. A. Aramendia, A. Marinas, J. M. Marinas, and F. J. Urbano, Appl. Catal. A : Gen. **306**, 120 (2006). https://doi.org/10.1016/j.apcata.2006.03.046